

Effect of f-c hybridization on the γ→α phase transition of cerium studied by lanthanum doping

Yong-Huang Wang(王永欢), Yun Zhang(张云), Yu Liu(刘瑜), Xiao Tan(谈笑), Ce Ma(马策), Yue-Chao Wang(王越超), Qiang Zhang(张强), Deng-Peng Yuan(袁登鹏), Dan Jian(简单), Jian Wu(吴健), Chao Lai(赖超), Xi-Yang Wang(王西洋), Xue-Bing Luo(罗学兵), Qiu-Yun Chen(陈秋云), Wei Feng(冯卫), Qin Liu(刘琴), Qun-Qing Hao(郝群庆), Yi Liu(刘毅), Shi-Yong Tan(谭世勇), Xie-Gang Zhu(朱燮刚), Hai-Feng Song(宋海峰), and Xin-Chun Lai(赖新春)

Citation: Chin. Phys. B, 2022, 31 (**8**): 087102. DOI: 10.1088/1674-1056/ac7210
Journal homepage: http://cpb.iphy.ac.cn; http://iopscience.iop.org/cpb

What follows is a list of articles you may be interested in

Pressure- and temperature-dependent luminescence from Tm^{3+} ions doped in $GdYTaO_4$

Peng-Yu Zhou(周鹏宇), Xiu-Ming Dou(窦秀明), Bao-Quan Sun(孙宝权), Ren-Qin Dou(窦仁琴), Qing-Li Zhang(张庆礼), Bao Liu(刘鲍), Pu-Geng Hou(侯朴赓), Kai-Lin Chi(迟凯邺), and Kun Ding(丁琨)
Chin. Phys. B, 2022, 31 (**1**): 017101. DOI: 10.1088/1674-1056/ac0526

Ultra-low Young's modulus and high super-exchange interactions in monolayer CrN: A promising candidate for flexible spintronic applications

Yang Song(宋洋), Yan-Fang Zhang(张艳芳), Jinbo Pan(潘金波), and Shixuan Du(杜世萱)
Chin. Phys. B, 2021, 30 (**4**): 047105. DOI: 10.1088/1674-1056/abdb20

Two-dimensional electron gas characteristics of InP-based high electron mobility transistor terahertz detector

Jin-Lun Li(李金伦), Shao-Hui Cui(崔少辉), Jian-Xing Xu(徐建星), Xiao-Ran Cui(崔晓然), Chun-Yan Guo(郭春妍), Ben Ma(马奔), Hai-Qiao Ni(倪海桥), Zhi-Chuan Niu(牛智川)
Chin. Phys. B, 2018, 27 (**4**): 047101. DOI: 10.1088/1674-1056/27/4/047101

Cubic ZnO films obtained at low pressure by molecular beam epitaxy

Wang Xiao-Dan, Zhou Hua, Wang Hui-Qiong, Ren Fei, Chen Xiao-Hang, Zhan Hua-Han, Zhou Ying-Hui, Kang Jun-Yong
Chin. Phys. B, 2015, 24 (**9**): 097106. DOI: 10.1088/1674-1056/24/9/097106

Characterization of deep acceptor level in as-grown ZnO thin film by molecular beam epitaxy

M. Asghar, K. Mahmood, M. A. Hasan, I. T. Ferguson, R. Tsu, M. Willder
Chin. Phys. B, 2014, 23 (**9**): 097101. DOI: 10.1088/1674-1056/23/9/097101

RAPID COMMUNICATION

Effect of f–c hybridization on the $\gamma \rightarrow \alpha$ phase transition of cerium studied by lanthanum doping

Yong-Huan Wang(王永欢)[1,†], Yun Zhang(张云)[1,†], Yu Liu(刘瑜)[2,†], Xiao Tan(谈笑)[1], Ce Ma(马策)[1], Yue-Chao Wang(王越超)[2], Qiang Zhang(张强)[1], Deng-Peng Yuan(袁登鹏)[1], Dan Jian(简单)[1], Jian Wu(吴健)[1], Chao Lai(赖超)[1], Xi-Yang Wang(王西洋)[1], Xue-Bing Luo(罗学兵)[1], Qiu-Yun Chen(陈秋云)[1], Wei Feng(冯卫)[1], Qin Liu(刘琴)[1], Qun-Qing Hao(郝群庆)[1], Yi Liu(刘毅)[1], Shi-Yong Tan(谭世勇)[1], Xie-Gang Zhu(朱燮刚)[1,‡], Hai-Feng Song(宋海峰)[2,§], and Xin-Chun Lai(赖新春)[1,¶]

[1] *Science and Technology on Surface Physics and Chemistry Laboratory, Jiangyou* 621908, *China*
[2] *Laboratory of Computational Physics, Institute of Applied Physics and Computational Mathematics, Beijing* 100088, *China*

(Received 10 April 2022; revised manuscript received 9 May 2022; accepted manuscript online 23 May 2022)

The hybridization between the localized 4f level (f) with conduction (c) electrons in γ-Ce upon cooling has been previously revealed in single crystalline thin films experimentally and theoretically, whereas its influence on the $\gamma \rightarrow \alpha$ phase transition was not explicitly verified, due to the fact that the phase transition happened in the bulk-layer, leaving the surface in the γ phase. Here in our work, we circumvent this issue by investigating the effect of alloying addition of La on Ce, by means of crystal structure, electronic transport and angle resolved photoemission spectroscopy measurements, together with a phenomenological periodic Anderson model and a modified Anderson impurity model. Our current researches indicate that the weakening of f–c hybridization is the major factor in the suppression of $\gamma \rightarrow \alpha$ phase transition by La doping. The consistency of our results with the effects of other rare earth and actinide alloying additions on the $\gamma \rightarrow \alpha$ phase transition of Ce is also discussed. Our work demonstrates the importance of the interaction between f and c electrons in understanding the unconventional phase transition in Ce, which is intuitive for further researches on other rare earth and actinide metals and alloys with similar phase transition behaviors.

Keywords: structural phase transition, molecular beam epitaxy, ARPES, f-electron system

PACS: 71.27.+a, 64.60.–i, 79.60.–i, 81.15.–z **DOI:** 10.1088/1674-1056/ac7210

1. Introduction

Among the f electron systems, i.e., lanthanide and actinide metals, alloys and intermetallic compounds, cerium has its unique importance, in the sense that it is the first element possessing one f electron and serves as the prototypical system in exploring the fascinating properties of f electrons. Historically, cerium metal has been attracting the attention of researchers due to its complex phase transition under moderate pressure and temperature conditions, in which it is believed that its single f electron has been playing important roles. Face-centered cubic (FCC) γ-phase cerium will transform into the same FCC α-phase, with an unconventional volume collapse of up to 16.5%, under a moderate pressure of ~ 0.78 GPa at ambient temperature, or cooled down to low temperature ($\sim 141 \pm 10$ K for bulk materials,[1] or down to around 50 K for single crystalline thin films[2]) at ambient pressure. As for the explanation of the mechanism of this intriguing phase transition, among the various theoretical models, i.e., the promotional model,[3–5] the Mott transition model[6] and the Kondo volume collapse (KVC) model,[7,8] the last one seems to be more adequate. In the KVC model, it is believed that the increase of hybridization between f electrons and conduction electrons drives the $\gamma \rightarrow \alpha$ phase transition in Ce metal, and strong f–c hybridization has been revealed in the band structures of single crystalline Ce thin films characterized by high resolution angle resolved photoemission spectroscopy (ARPES) experiments.[2,9,10] However, direct experimental observation of the band dispersions of α-Ce has not been achieved, due to the incompleteness of the $\gamma \rightarrow \alpha$ phase transition and persistent existence of γ phase on the surface of Ce thin films, which makes the identification of f–c hybridization evolution and the role it playing across the $\gamma \rightarrow \alpha$ phase transition ambiguous. Therefore, approaches that could manipulate the f–c hybridization and investigate its effects on the $\gamma \rightarrow \alpha$ phase transition are demanded.

For the purpose of determining the relationship between phase (atomic arrangement, basically) and electronic properties, pressure is one important variable.[11] It is plausible that only moderate hydrostatic pressure is needed to manipulate the $\gamma \rightarrow \alpha$ phase transitions in Ce, however, photoemission is

[†]These authors contributed equally to this work.
[‡]Corresponding author. E-mail: zhuxiegang@caep.cn
[§]Corresponding author. E-mail: song_haifeng@iapcm.ac.cn
[¶]Corresponding author. E-mail: laixinchun@caep.cn

© 2022 Chinese Physical Society and IOP Publishing Ltd

technically non-applicable for hydrostatic pressurized solids. Another commonly adopted variable is alloying doping, which has been usually termed as chemical pressure. The effects on the $\gamma \rightarrow \alpha$ phase transition of Ce by doping with some rare earth and actinide elements have been studied by dilatometric and x-ray techniques.[12,13] However, studies on the evolution of the electronic structure are still lacking. Among the various alloying dopants, La is one of a kind, with the reasons as follows: (1) with non-f electron occupancy, La acts as non-magnetic ion, which could effectively tune the concentration of the localized f electron of Ce; (2) Ce and La alloyed in arbitrary chemical ratio could maintain the FCC structure in thin films; (3) La doping expands the FCC lattice as its concentration increases, from 5.16 Å for Ce[14] to 5.31 Å for La,[15] resulting in an effective negative chemical pressure. Here in our work, we have successfully grown $Ce_{1-x}La_x$ thin films by molecular beam epitaxy (MBE), with La concentration x being tuned continuously from zero to 100%. Lattice structure characterization reveals that the thin films were in the FCC structure and the effective negative pressure was realized by La doping. Suppression of $\gamma \rightarrow \alpha$ phase transition by La doping was directly confirmed by electronic transport measurements. High resolution band structures of $Ce_{1-x}La_x$ thin films were obtained by ARPES, confirming that the electronic structure of 4f electron in Ce could be effectively modified by La doping. The evolution of f–c hybridization by La doping was investigated by both a phenomenological periodic Anderson model (PAM) and a modified Anderson impurity model [the Gunnarsson–Schönhammer (GS) model]. We show that the change in f–c hybridization correlates with the suppression of $\gamma \rightarrow \alpha$ phase transition in Ce, which is consistent with the scenario of the KVC model.

2. Experimental methods

$Ce_{1-x}La_x$ thin films were grown by MBE. High purity Ce and La metals (99.9%) were used and thoroughly degassed at 1600 °C and 1500 °C separately before thermal evaporation. La concentration x was controlled by finely tuning the flux ratio of Ce and La during the thermal evaporation. Quartz crystal micro-balance was used to calibrate the flux rate of Ce and La down to an accuracy within 0.002 Å/s. Single crystalline $Ce_{1-x}La_x$ thin films were deposited on conductive graphene/6H-SiC(0001) substrate for *in-situ* band structure characterization, while polycrystalline thin films were grown on insulating Al_2O_3(11-20) substrate for *ex-situ* x-ray diffraction (XRD) and electronic transport measurements. For the photoemission spectroscopy (PES) experiment, the photoelectrons were excited by the He Iα (21.2 eV) resonance line of a commercial helium gas discharge lamp. The light was guided to the analysis chamber by a quartz capillary. In virtue of the efficient three-stage differential pumping system, the pressure in the analysis chamber was lower than 1×10^{-10} mbar during our experiments, satisfying the harsh criteria for probing the physical properties of chemically high-reactive elements. A VG Scienta R4000 energy analyzer was used to collect the photoelectrons. The total energy and momentum resolutions were better than 10 meV and 0.006 $Å^{-1}$, respectively. The transport measurements were performed with the standard four-probe technique using a physical property measurement system (PPMS-9). Pure indium (5N) metal was used to make the electrode contacts. The resistivity versus temperature curves were recorded during a cooling and warming cycle, respectively. It should be noted that different samples with different La concentrations were used in the above experiments to cover a wide range of La concentration. Theoretical methods will be discussed in more detail in the following main context.

3. Results

3.1. Lattice structure and transport properties

RHEED pattern of an as-grown $Ce_{0.50}La_{0.50}$ thin film on graphene/6H-SiC(0001) substrate is demonstrated in Fig. 1(a), with incident electron direction along $[1\bar{1}0]$. The RHEED pattern shows that the thin film has no surface reconstruction or multi-domain region other than the (111)-orientated single crystalline termination. And the sharp streaks also indicate the high quality of the surface morphology. The intensities of the diffracted electrons within the red dashed box in Fig. 1(a) were integrated along the vertical direction and recorded every two seconds during the growth, which are summarized in Fig. 1(b). The in-plane lattice constant a of the thin film could be calculated by comparing the spacings of the RHEED streaks of the thin film with that of the substrate, and the calculated a is 3.695 ± 0.005 Å for $Ce_{0.50}La_{0.50}$. We have calculated a for various $Ce_{1-x}La_x$ single crystalline thin films, as shown in Fig. 1(c). The overall increasing trend of the in-plane lattice constant as La doping increases is obvious, which is consistent with the fact that La doping would expand the lattice of Ce.[14,15] The error bars are mainly from the resolution of our CCD camera, and thus are fixed at ±0.005 Å for all the data points. As for pure Ce and La single crystalline thin films, the calculated lattice parameters for FCC structure are simply $\sqrt{2}a_0$, and are 5.173 ± 0.005 Å and 5.331 ± 0.005 Å, respectively.

Polycrystalline $Ce_{1-x}La_x$ samples with the thickness of ~ 1 μm were used for transport measurement. XRD analysis was conducted just after the samples were taken out of the MBE chamber, as demonstrated in Fig. 1(d). The values of 2θ have been calibrated by the (110) and (220) peaks of the Al_2O_3 substrate, and the intensities have been renormalized by the intensity of pure Ce (111) peak for a better view. According to

the standard PDF cards, we know the Ce film (red curve in Fig. 1(d)) corresponds to γ-Ce of FCC crystal structure. The strong intensity of the (111) peaks for all the samples except pure La film indicates that the samples were highly oriented in the [111] crystallographic direction. However, the *in-situ* reflected high-energy electron diffraction (RHEED) showed that all the films grown on Al_2O_3(11-20) substrates were polycrystalline, which means that the films were mainly consisted with crystallites oriented along [111] out of plane and randomly in-plane. The case for pure La film was quite different: the (111) peak was much weaker relative to that of the substrate, and the signal to noise ratio was much lower than that of the Ce film, indicating that the crystallites in the La film were totally randomly oriented. The evolution of the lattice parameters could be seen from the continuous shift of the (111) and (222) peaks between the vertical lines in Fig. 1(d), and in more detail in Fig. 1(e), demonstrating the linear expansion of the lattices by La doping. It should be stressed that the lattice parameters of our pure Ce and La polycrystalline thin films, i.e., 5.166 ± 0.002 Å and 5.307 ± 0.005 Å, corresponded to their FCC structures,[14,16] respectively, and are consistent with our RHEED experiment results.

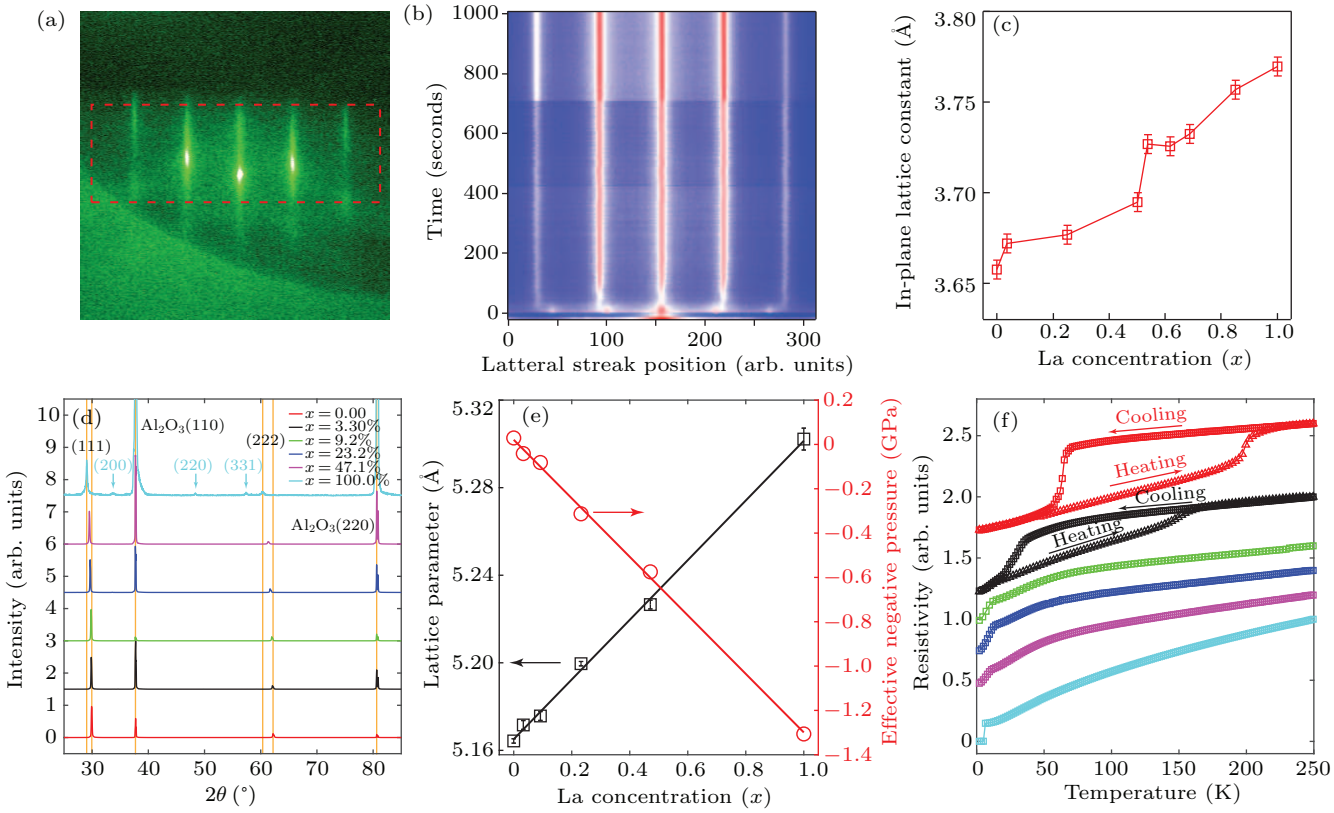


Fig. 1. (a) RHEED patterns of $Ce_{0.50}La_{0.50}$ thin film taken with incident electron directions along $[1\bar{1}0]$; (b) evolution of the RHEED streaks during the growth as a function of time; (c) in-plane lattice constants of various $Ce_{1-x}La_x$ single crystalline thin films; (d) renormalized XRD curves of polycrystalline $Ce_{1-x}La_x$ thin films; (e) the evolution of lattice parameters in the FCC structure and the effective negative pressures by La doping; (f) normalized resistivity as a function of temperature.

The pressure to volume (P–V) relationship of pure Ce was almost linear for pressures lower than ~ 0.70 GPa.[17,18] Therefore, in order to investigate the negative pressure effect by La doping, we could linearly extrapolate the P–V relationship of pure Ce to negative pressure. Based on our experimental lattice parameters, the effective negative pressures for various La concentrations were calculated and shown in Fig. 1(e).

The resistivity of the above $Ce_{1-x}La_x$ samples was renormalized by their values at 250 K and shown in Fig. 1(f). Hysteresis loops were observed in pure Ce and $Ce_{0.967}La_{0.033}$ thin films, which are the characteristic feature of the $\gamma \rightarrow \alpha$ phase transition. The area enclosed by the hysteresis loop shrank a lot by 3.30% La doping, and diminished for La concentration at 9.20% and above, which means that the $\gamma \rightarrow \alpha$ phase transition was suppressed by a few percentage of La doping, i.e., less than 10% of La concentration. It should be noted that the lattice expansion for x less than 10% was smaller than $\sim 0.2\%$, which is almost negligible. Thus, the mechanism of the suppression of the phase transition lies somewhere else, where the electronic properties of the f electrons and their interaction with conduction electrons might be playing important roles.

3.2. Photoemission studies

Detailed studies on the electronic structures of pure Ce thin films by ARPES could be found in Refs. [2,9,10]. The ARPES spectra for our as-grown $Ce_{1-x}La_x$ thin films with var-

ious La concentrations are shown in Fig. 2, corresponding to the spectra taken along K–Γ–K in the surface Brillouin zone (SBZ). Figure 2(a) shows the main features of the band structures of the Ce thin film: three dispersive bands that are originated from non-f electrons (s, p, d), labeled as α, β and γ, respectively; three non-dispersive bands that locate near Fermi level ($E_{\rm F}$), ~ 250 meV and ~ 2 eV below $E_{\rm F}$, which were conventionally attributed to the $4f^1_{5/2}$, $4f^1_{7/2}$ and $4f^0$, respectively. The clear presence of the $4f^1$ levels near $E_{\rm F}$ indicates the strong hybridization between conduction electrons with the 4f-electron in cerium, enhancing its spectral intensity near $E_{\rm F}$. As for pure La thin film, the ARPES spectrum in Fig. 2(h) shows almost identical dispersive bands as observed in Ce, with the non-dispersive f bands missing, which is a consequence of the absence of f-electron in La. With increasing La concentration in $Ce_{1-x}La_x$, the 4f bands faded continuously and the conduction bands remained similar, as shown in Figs. 2(b)–2(g).

To investigate the k-dependent f–c hybridization, we introduce the phenomenological periodic Anderson model (PAM), which gives the band dispersion describing the hybridization as[2,19,20]

$$E_k^{\pm} = \frac{\varepsilon_0 + \varepsilon(k) \pm \sqrt{(\varepsilon_0 - \varepsilon(k))^2 + 4|V_k|^2}}{2}. \quad (1)$$

Here ε_0 is the 4f ground state energy, which is not k-dependent. $\varepsilon(k)$ is the valence band dispersion at room temperature, which is parabolic and concave down,[2] as shown by the black curves in Figs. 3(a)–3(c). And V_k is the renormalized hybridization strength. When the La concentration x is below 61.7%, all band structures around the Fermi level of the Ce–La alloys can be fitted with the PAM, as shown in Figs. 3(a)–3(c). Without regard to the f–c hybridization, only conduction band crosses the Fermi level (see the black lines). When the hybridization strengthens, the conduction band bends to another direction with much smaller Fermi velocities (see the red dots) and this is how the heavy electrons emerge. However, we find that the f–c hybridization gap of the Ce–La alloys decreases as the La concentration increases as shown in Fig. 3(h) and the green marker line in Fig. 3(g), indicating the decreased hybridization strength. Furthermore, when the La concentration is 61.7% or more, as shown in Fig. 3(d), the valence band structure cannot be fitted with the PAM, namely, the hybridization effect disappears, mainly resulted from the faint f bands. That is to say, the hybridization strength of the Ce–La alloys monotonously decreases as the La concentration increases until its disappearance.

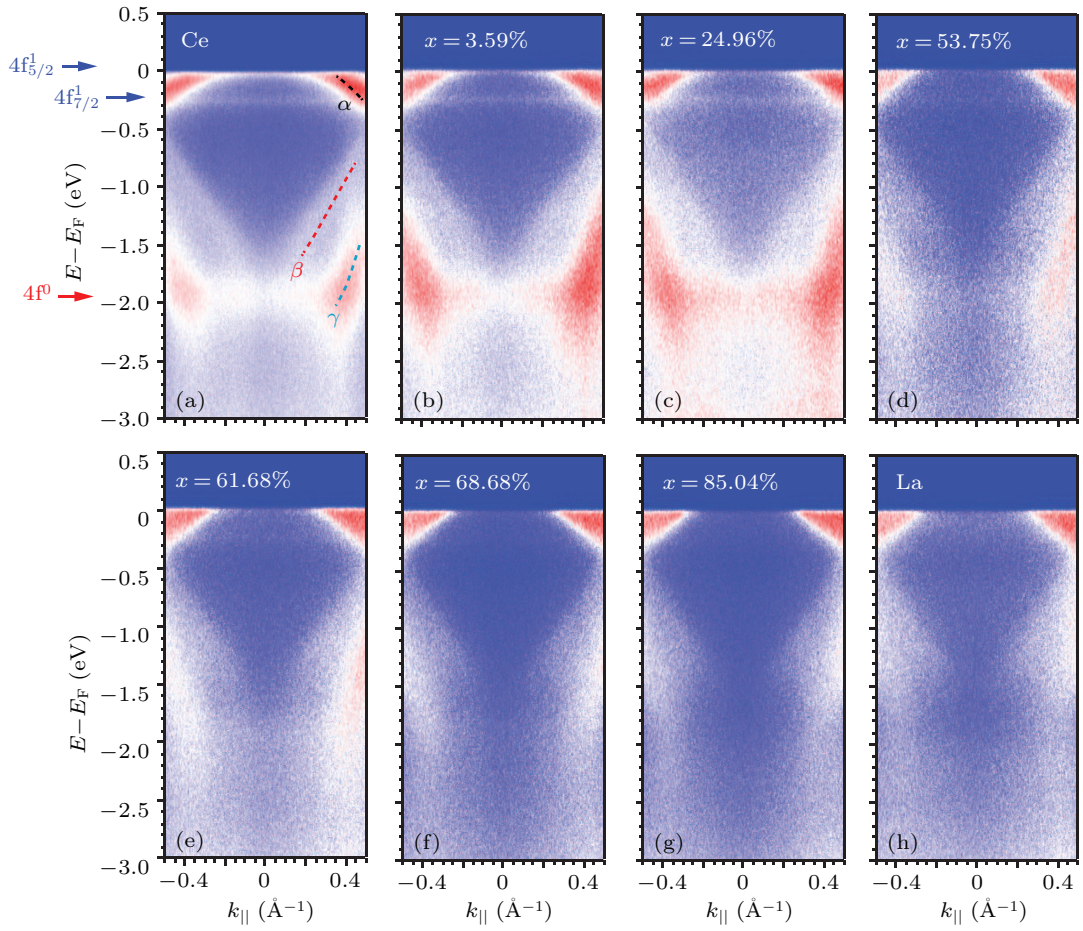


Fig. 2. (a)–(h) ARPES spectra within large energy scale (from −3.0 eV to 0.5 eV) for $Ce_{1-x}La_x$ alloy thin films along K–Γ–K in the surface Brillouin zone for various La concentrations.

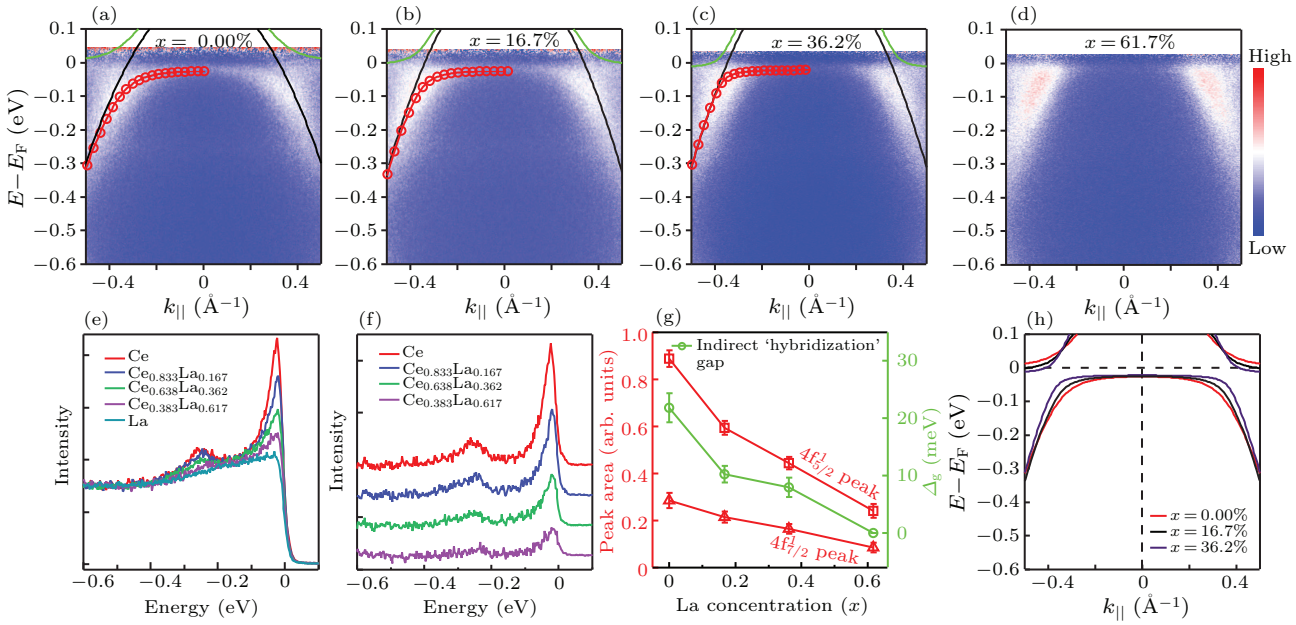


Fig. 3. (a)–(d) Detailed band dispersions of Ce, $Ce_{0.833}La_{0.167}$, $Ce_{0.638}La_{0.362}$ and $Ce_{0.383}La_{0.617}$ thin films along K–Γ–K, in which the f–c hybridization bands are fitted by PAM model. The red dotted lines and green lines are the fitted results, while the black lines are the conduction band dispersions without f–c hybridization. All the PAM fitting results from (a) to (c) are also summarized in (h). (e) Normalized EDCs within ± 0.04 Å around the Γ point of the thin films in (a)–(d), together with that of pure La thin film (ARPES spectra not shown here). (f) Normalized EDCs of (a)–(d) in (e) subtracted that of pure La thin films. The spectra are vertically shifted for a better view. (g) Peak areas of $4f^1_{5/2}$ (open squares) and $4f^1_{7/2}$ (open triangles) fitted from (f), together with the fitted indirect hybridization gaps Δ_g (open circles).

Additionally, we also analyzed the evolution of the f band intensities with La doping, which was done by investigating the energy distribution curves (EDCs) of the spectra. The EDC peak intensities of both $4f^1_{5/2}$ and $4f^1_{7/2}$ bands gradually decrease as the La concentration increases as shown in Figs. 3(e) and 3(f). This phenomenon is quite similar to the f band evolutions of the Ce film as a function of temperature and mainly results from the localization of f electrons with increasing temperature. We can also find that the $4f^1_{5/2}$ and $4f^1_{7/2}$ peak areas of the EDCs decrease with increasing La concentration as shown in Fig. 3(g). When the f electron concentration is extremely low [see EDC of $Ce_{0.383}La_{0.617}$ in Figs. 3(e) and 3(f)], there still have some $4f^1_{5/2}$ intensities around the Fermi level. However, the f–c hybridization does not happen and the band dispersion cannot be fitted with the PAM as shown in Fig. 3(d). With the increasing f electron concentration, the intensity of f band strengthens and the f–c hybridization also emerges as shown in Figs. 3(a)–3(c).

3.3. Theoretical consideration

From the above photoemission results, we could see the persistent existence of f–c hybridization in $Ce_{1-x}La_x$ at low temperature for La concentrations over quite a large range. And the hybridization effect could be well demonstrated by the phenomenological PAM, even La doping could have driven the 4f electrons from the Kondo lattice to the single impurity configuration. Therefore, it is intriguing and informative to investigate the electronic behaviors of $Ce_{1-x}La_x$ alloys in the impurity model. In the work of Gunnarsson and Schönhammer, the electron spectroscopies of Ce related compounds, including the x-ray photoemission, 3d→4f x-ray absorption, the valence photoemission, and the bremsstrahlung isochromat spectra, have been calculated in a modified Anderson impurity model.[21] This so-called GS model has been well verified in its applications in a series of Ce compounds.[22,23] Here in our work, we have applied the GS model to simulate the photoemission spectra of our samples. To simulate the three peaks structure ($4f^0$, $4f^1_{7/2}$ and $4f^1_{5/2}$ of the photoemission spectra of Ce related materials), the spin–orbit splitting of the f level was include in the GS model, and the resultant valence photoemission spectra could be described analytically in the first-order approximation as follows:

$$\rho_v(\varepsilon) = A^2 \int d\varepsilon' \left|V(\varepsilon')\right|^2 \left[\frac{N_{f1}}{(\Delta E - \varepsilon_f + \varepsilon')^2} + \frac{N_{f2}}{\left(\Delta E - \varepsilon_f - \Delta\varepsilon_f + \varepsilon'\right)^2}\right] \times \tilde{g}(z - \Delta E + \varepsilon_f - \varepsilon'), \quad (2)$$

where $V(\varepsilon)$ describes the hopping between the f level and the conduction states, and is related to the coupling strength Δ by $\Delta = \pi \max_\varepsilon[|V(\varepsilon)|^2]$. N_{f1} and N_{f2} are the degeneracy of the $j = 7/2$ and $j = 5/2$ levels, i.e., 8 and 6, respectively. ΔE is the lowering of the energy when the f electron impurity is introduced, and could be calculated numerically. ε_f and $\Delta\varepsilon_f$ are the position and the spin–orbit splitting of the f level, respectively. The definition of $\tilde{g}$ could be found in the appendix of the literature.[21] To numerically calculate $\rho_v(\varepsilon)$, an infinitesimal 0^+ was introduced ($z = \varepsilon - i0^+$) in the integration procedure,

and the imaginary part of the integration corresponds to the valence photoemission spectra.

As for $|V(\varepsilon)|^2$, instead of using the over-simplified semi-elliptical form,[21] we have adopted a double-peaked Lorentzian line-shape to account for the coupling between the f level and different conduction bands. As is well known, the matrix element effect would induce different photoemission spectra for various photon energies, which was not explicitly included in the GS model. However, it should be noted that the normal emission spectra of our $Ce_{1-x}La_x$ samples resemble the resonance photoemission results of Ce, especially for pure Ce thin films.[2] Therefore, we could approximately simulate our experimental spectra as a combination of the total spectral weight of f-electron (regardless of the matrix element effect), and the contribution from the conduction bands, which is related to the linear combination of the Lorentzian peaks in $|V(\varepsilon)|^2$. Additionally, the background is simulated by a quadratic curve, which corresponds to the systematic noise and the second order photoelectrons. During the fitting procedure, the spin–orbit splitting $\Delta\varepsilon_f$ was fixed at 280 meV.[24,25] The starting values of Δ and ε_f were 0.125 eV and -1.2 eV, respectively. A Fermi–Dirac distribution (FDD) of 80 K was also introduced, which corresponds to the experimental temperature. All the fitting parameters were constrained in reasonable ranges in order to guarantee that the results have physical meaning.

The experimental valence spectra were extracted from Fig. 2 by integrating the EDCs within ± 0.50 Å^{-1} around the Γ point, and were further smoothed by the multicomponent function as mentioned in Ref. [2]. The resultant smoothed spectra are demonstrated as solid lines in Fig. 4(a). The dotted lines in Fig. 4(a) are the fitted valence spectra by the GS model. The overall fittings are quite satisfactory for La concentration below 53.75%, where the location, relative intensities and shape of the $4f^0$ ionization peak, the Kondo peak near E_F and its $4f^1_{7/2}$ spin–orbit splitting duplicate are well reproduced. As the La concentration increases further, the spectral intensity of the normal conduction band feature [indicated by the vertical arrows in Fig. 4(a)] gradually prevails that of the $4f^0$ peak, and the fitting results deviate from the experimental spectra below -1.5 eV. As mentioned above, the overall fitted spectrum is composed by the background and contributions from f-electron and conduction bands, which could be extracted separately during our fitting procedure. To have a better view of the evolutions from various contributions, we took pure Ce and La concentration $x = 24.96\%$ as examples and extracted the background, f-electron and conduction bands, as shown in Fig. 4(b). We could see that the backgrounds (dashed black curves in Fig. 4(b)) show similar behavior, while the spectral contributions from f-electron and conduction bands demonstrate obvious variations. For the f-electron spectra (dashed red curves in Fig. 4(b)), the intensity ratio of the $4f^0/4f^1$ for $x = 24.96\%$ is bigger than that of pure Ce, which means that the f-electron occupancy is higher for $x = 24.96\%$. Additionally, the increase of the spectral weight of the conduction bands (dashed green curves in Fig. 4(b)) reveals the increasing contributions from La. The f electron occupancy n_f could be calculated by integrating the square of the module of the wave functions of the states when the f electron impurity was introduced in the ground state.[21] The calculated f electron occupancy for pure Ce is approximate 0.86, and increases to ~ 0.90 for $x = 24.06\%$, as shown in Fig. 4(c). The increase of n_f indicates that the f electrons in $Ce_{1-x}La_x$ become more localized, or in other word, the coupling strength of the f level with the conduction states weakens, which is consistent with the previous discussed PAM fitting results of the f–c hybridization. However, the relationship between n_f and x changes as x goes beyond 24.96%, i.e., n_f decreases monotonically as x increases, as shown in Fig. 4(c). This could be attributed to the fact that the valence spectra demonstrate more and more La features as x increases, and Ce atoms act as dopant instead of host, in which cases the GS model seems to be not adequate. Similar behaviors were also observed for the coupling strength Δ, as shown by the red marker line in Fig. 4(c), despite that Δ decreased with La concentration up to 53.75%.

As mentioned above, the central idea of the GS model originated from the impurity Anderson model, and the coupling of f-level with conduction states resulted in the 3-peak feature ($4f^0$, $4f^1_{5/2}$ and $4f^1_{7/2}$) in the valence spectra of many Ce related materials. For the validity of this model, the screening of the local momentum of f electrons by the conduction electrons should be moderate, and the lattice structure of Ce should be intact to ensure the formation of f bands. La doping, on one hand, would effectively increase the ratio of conduction electrons to f electrons, i.e., strengthening the screening of f electron, and on the other hand, would gradually destroy the original Ce lattice, both of which could drive the system from strong f–c coupling to weak coupling, and eventually to no coupling. Additionally, according to the previous XRD results, La doping gradually expands the FCC lattice, exerting effective negative pressure on the lattice, which would also weaken the hybridization between f and conduction electrons, despite the fact that its effect is negligible for a few percentage of La doping. Therefore, we could safely conclude that the suppression of $\gamma \rightarrow \alpha$ phase transition is mainly due to the weakening of f–c hybridization, and on the contrary, the strengthening of f–c hybridization could drive the $\gamma \rightarrow \alpha$ phase transition upon the condition of cooling or positive pressure.

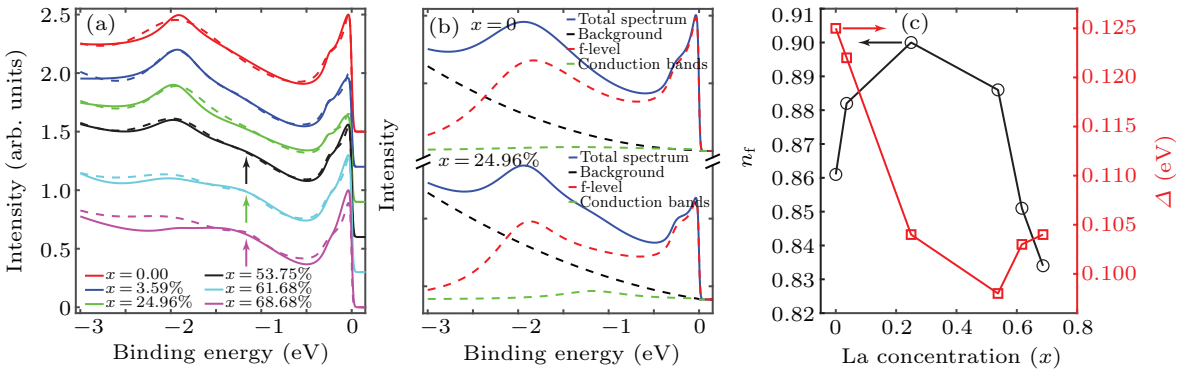


Fig. 4. (a) Experimental (solid lines) and fitted (dotted lines) valence photoemission spectra of $Ce_{1-x}La_x$ thin films; (b) detailed fitting results for pure Ce and La concentration $x = 24.96\%$, as shown in the upper and lower sections. The total fitted spectra, background, contributions from f-electron and conduction bands are demonstrated by solid blue, dashed black, red and green curves, respectively. (c) Calculated f electron occupancy n_f and fitted coupling strength Δ for various La concentration.

4. Discussion and conclusion

La doping in Ce has two major influences: diluting the f electron concentration and expanding the lattice parameters. Our researches have demonstrated that the former would greatly weaken the f–c hybridization effect, and consequently suppress the $\gamma \rightarrow \alpha$ phase transition in Ce upon cooling, or in other words, stabilize the γ phase. This indicates that greater pressure should be expected for the $\gamma \rightarrow \alpha$ phase transition to take place for La doped Ce samples at room temperature, which was indeed the case from the experimental results on bulk samples.[13] Additionally, many rare earth alloying additions on Ce, such as Sc, Pr, Dy and Lu, shrank the lattice by exerting positive chemical pressure and increased the phase transition pressure at room temperature.[12,13,26] One special alloying addition is the actinide element Pu, which also shrank the lattice from 0 up to $\sim 25\%$ concentration, whereas decreasing the transition pressure. This means that Ce is prone to phase transition upon Pu doping. It is well known that Ce and Pu are counterparts to each other,[27,28] in the sense that: on one hand, they both undergo huge volume collapse, 17% for Ce and 25% for Pu, across their $\gamma \rightarrow \alpha$ and $\delta \rightarrow \alpha$ phase transitions, respectively; and on the other hand, the 4f-electron of Ce and 5f-electron of Pu both have dual itinerant and localized behaviors, demonstrating strong many-body effects and strong interaction with their conduction electrons. We conjecture that Pu doping would strengthen the f–c hybridization, whereas other alloying additions would not. Another interesting alloying addition is Th, which also shrank the FCC lattice of Ce, however, the pressure needed for the $\gamma \rightarrow \alpha$ phase transition at room temperature only decreased slightly, with a value of $\sim 3.6\%$ at 20% of Th doping, compared with the value of $\sim 71.5\%$ for 20% of Pu doping.[12,13] What is more, the $\gamma \rightarrow \alpha$ phase transition persistently existed upon cooling for a large range of Th doping from 0 to 60%. Despite the atomic ground state configuration $6d^27s^2$, Th metal in the FCC structure has a non-integer 5f-electron count due to the 5f–6d overlapping,[29] or in other word, f–c hybridization. Alloying the two elements most probably did not change the overall valence states and f-electron occupancy too much, thus Th doping had much smaller influence on the phase transition of Ce, compared with the other alloying elements.

To summarize, we have experimentally and theoretically investigated the effects of alloying addition on Ce by La. Lattice structure and electronic transport experiments have revealed linear expansion of the FCC lattice and suppression of the $\gamma \rightarrow \alpha$ phase transition. Detailed ARPES measurements and theoretically model calculations have demonstrated the weakening of f–c hybridization and the important role it played in the suppression of the $\gamma \rightarrow \alpha$ structural phase transition. Our results provoke further studies on the electronic origins of the phase transitions and phase stabilities of rare earth and actinide metals and alloys.

Acknowledgements

Project supported by the National Key Research and Development Program of China (Grant Nos. 2021YFA1601100 and 2017YFA0303104), the SPC-Lab Research Fund (Grant No. WDZC201901), the Science Challenge Project (Grant Nos. TZ2016004 and TZ2018002), the National Natural Science Foundation of China (Grant Nos. U1630248, 11774320, and 11904334), Special Funds of Institute of Materials (Grant No. TP02201904), and the Development Funds (Grant No. JZX7Y201901SY00900107).

References

[1] Koskenmaki D Cand Gschneidner K A 1978 *Handbook on the Physics and Chemistry of Rare Earths*, Vol. 1, Chapter 4: Cerium (Elsevier) pp. 337–377
[2] Zhu X G, Liu Y, Zhao Y W, Wang Y C, Zhang Y, Lu C, Duan Y, Xie D H, Feng W, Jian D, Wang Y H, Tan S Y, Liu Q, Zhang W, Liu Y, Luo L Z, Luo X B, Chen Q Y, Song H F and Lai X C 2020 *npj Quantum Mater.* **5** 47
[3] Coqblin B and Blandin A 1968 *Adv. Phys.* **17** 281
[4] Ramirez R and Falicov L M 1971 *Phys. Rev. B* **3** 2425
[5] Hirst L L 1974 *J. Phys. Chem. Solids* **35** 1285
[6] Johansson B 1974 *Philos. Mag.* **30** 469
[7] Allen J W and Martin R M 1982 *Phys. Rev. Lett.* **49** 1106

[8] Allen J W and Liu L Z 1992 *Phys. Rev. B* **46** 5047

[9] Chen Q Y, Feng W, Xie D H, Lai X C, Zhu X G and Huang L 2018 *Phys. Rev. B* **97** 155155

[10] Wu Y, Fang Y, Li P Xiao Z, Zheng H, Yuan H Q, Cao C, Yang Y F and Liu Y 2021 *Nat. Commun.* **12** 2520

[11] Drickamer H G 1963 *Science* **142** 1429

[12] Gschneidner K A, Elliott R O and McDonald R R 1962 *J. Phys. Chem. Solids* **23** 1191

[13] Gschneidner K A, Elliott R O and McDonald R R 1962 *J. Phys. Chem. Solids* **23** 1201

[14] Nikolaev A V and Tsvyashchenko A V 2012 *Phys.-Uspekhi* **55** 657

[15] Syassen K and Holzapfel W B 1975 *Solid State Commun.* **16** 533

[16] BağcıS, Tütüncü H M, Duman S and Srivastava G P 2010 *Phys. Rev. B* **81** 144507

[17] Decremps F, Belhadi L, Farber D L, Moore K T, Occelli F, Gauthier M, Polian A, Antonangeli D, Aracne-Ruddle C M and Amadon B 2011 *Phys. Rev. Lett.* **106** 065701

[18] Ma C, Dou Z Y, Zhu H Y, Fu G Y, Tan X, Bai B, Zhang P C and Cui Q L 2016 *Chin. Phys. B* **25** 046401

[19] Chen Q Y, Xu D F, Niu X H, Jiang J, Peng R, Xu H C, Wen H P, Ding Z F, Huang K, Shu L, Zhang Y J, Lee H, Strocov V N, Shi M, Bisti F, Schmitt T, Huang Y B, Dudin P, Lai X C, Kirchner S, Yuan H Q and Feng D L 2017 *Phys. Rev. B* **96** 045107

[20] Chen Q Y, Tan S Y, Feng W, Luo L Z, Zhu X G and Lai X C 2019 *Chin. Phys. B* **28** 077404

[21] Gunnarsson O and Schönhammer K 1983 *Phys. Rev. B* **28** 4315

[22] Gunnarsson O and Schönhammer K 1983 *Phys. Rev. Lett.* **50** 604

[23] Patthey F, Imer J M, Schneider W D, Beck H, Baer Y and Delley B 1990 *Phys. Rev. B* **42** 8864

[24] Buchanan R A, Rast H E and Caspers H H 1966 *J. Chem. Phys.* **44** 4063

[25] Patthey F, Delley B, Schneider W D and Baer Y 1985 *Phys. Rev. Lett.* **55** 1518

[26] Shunk F A 1969 *Constitution of binary alloys, second supplement* (New York: McGraw-Hill)

[27] Moore K T and van der Laan G 2009 *Rev. Mod. Phys.* **81** 235

[28] Clark D L, Geeson D A and Hanrahan R J 2019 *Plutonium Handbook* (American Nuclear Society)

[29] Johansson B, Ahuja R, Eriksson O and Wills J M 1995 *Phys. Rev. Lett.* **75** 280